Scanning tunneling microscopy contrast of isovalent impurities on the GaAs (110) surface explained with a geometrical model

F. J. Tilley,[1] Mervyn Roy,[1,*] P. A. Maksym,[1] P. M. Koenraad,[2] C. M. Krammel,[2] and J. M. Ulloa[3]

[1]*Department of Physics and Astronomy, University of Leicester, University Road, Leicester LE1 7RH, United Kingdom*

[2]*COBRA Inter-University Research Institute, Department of Applied Physics, Eindhoven University of Technology, P.O. Box 513, NL-5600 MB Eindhoven, Netherlands*

[3]*Institute for Systems based on Optoelectronics and Microtechnology, Universidad Politécnica de Madrid, 28040 Madrid, Spain*

(Received 30 March 2015; published 27 January 2016)

Theoretical scanning tunneling microscopy (STM) images for all group-III and -V dopants on the GaAs (110) surface are calculated using density functional theory (DFT). In addition, a geometrical model based on the covalent radii of the dopants and substrate atoms is used to interpret the images. We find that the covalent radius of the dopant determines the geometry of the surface, which in turn determines the contrast seen in the STM images. Our model allows bond lengths to be predicted with an error of less than 4.2% and positions to be predicted with an average deviation of only 0.19 Å compared to positions from fully relaxed DFT. For nitrogen we demonstrate good qualitative agreement between simulated and experimental STM images for dopants located in the first three surface layers. We are able to explain differences in both the contrast and positions of bright and dark features in the STM image based on our geometrical model. We then provide a detailed quantitative analysis of the positions of the bright features for nitrogen dopants in the second layer. The agreement of the DFT calculation with experiment is excellent, with the positions of the peaks in simulated and experimental STM scans differing by less than 2% of the lattice constant. For dopants other than nitrogen, we compare the calculated STM image contrast with the available experimental data and again find good agreement.

DOI: 10.1103/PhysRevB.93.035313

I. INTRODUCTION

Single atomic impurities have many important applications such as single-photon emitters [1] and quantum computing [2,3]. Cross-sectional scanning tunneling microscopy (XSTM) is often used to image single impurities near surfaces; however, interpretation of the images is not simple. The image contrast depends on both the geometry of the surface and its electronic structure, and it can be difficult to disentangle these two effects. Geometry is the dominant effect [4] in some cases; in others it is electronic structure [5], while sometimes geometry and electronic structure are of equal importance [6], but in some cases, including single atomic impurities, the relative importance of the two effects is not known [7]. The present work shows that geometry is the dominant effect in the case of isovalent impurities near the GaAs (110) surface.

Our analysis consists of three steps. First, we compute the atomic and electronic structure with density functional theory (DFT). Next, we use these data to simulate STM images, and finally, we interpret the physics with a geometrical model based on covalent radii. The covalent radius of an atom is a measure of its effective size in a situation where it bonds covalently to other atoms. The length of the covalent bond between two atoms is the sum of their covalent radii, and these radii are available in the literature [8]. The bond lengths found in this way agree with DFT bond lengths to within an error of less than 4.2%. In addition, when the bonding configuration of surface impurities remains nearly tetrahedral, the covalent radius approach allows the surface atomic positions to be found to an accuracy of about 0.19 Å *without* any input from DFT.

A very important part of our analysis is that we have simulated XSTM images for all impurities from groups III and V. The image contrast changes that occur on going down each of these columns of the periodic table are very well correlated with the effective size of the impurity atoms involved, as measured by their covalent radius. This observation, together with the excellent agreement of our geometrical model with DFT, leads to the conclusion that geometry is the dominant effect in determining the XSTM image contrast.

Isovalent impurities are ideal for investigating and understanding XSTM contrast because the physics is not complicated by charging effects. Recently, XSTM has been used to investigate single isovalent nitrogen impurities in and below the surface layer of a cleaved GaAs (110) surface [9]. The behavior of the surface and subsurface nitrogen impurities has been investigated qualitatively [10] with DFT simulations; however, there has been no quantitative analysis or detailed comparison to the experimental results. Nor has there been any detailed analysis of other isovalent impurities from groups III and V. The present work includes a quantitative comparison of peak positions in our own XSTM image of an N impurity in the second atomic layer: the observed positions agree with DFT to within 2%. In addition, the predicted contrast for all impurities from groups III and V is compared with the available data from the literature, and good qualitative agreement is found.

In Sec. II we outline the DFT calculations, and in Sec. III we introduce the geometrical model we use to understand the relaxed geometry and the key features in the calculated STM images. In Sec. IV we explain the experimental procedure, and then in Sec. V we go through the analysis of the results for nitrogen and then the other group-III and -V impurities. Finally, in Sec. VI we present a summary of our work.

*Corresponding author: mr6@le.ac.uk

II. CALCULATION

DFT calculations were performed using the local-density approximation (LDA). For our calculations we employed Fritz-Haber-Institute (FHI) norm-conserving pseudopotentials [11] and the ABINIT software package [12,13]. Simulations of the clean GaAs (110) surface were checked prior to the addition of the impurities and were found to agree with the standard experimental relaxations, with a surface displacement between the gallium and arsenic atoms $\Delta_{1,\perp}$ of 0.067 nm and a buckling angle θ of 30.37° [14]. We used a standard configuration of a seven-atomic-layer slab with a 12-Å vacuum gap [10,15], and the system was allowed to fully relax with a tolerance on the forces of 1×10^{-4} hartrees/bohr. The lattice constant of the simulated system a_0 was 5.53 Å, which, while lower than the experimental value, is expected for pseudopotential calculations [16]. In Sec. V, when comparing to experimental data, the systems are scaled so all cell dimensions are in units of the lattice constant.

For all impurity simulations a 126-atom supercell with a 3×3 surface periodicity was used, with a cutoff energy for the plane-wave basis set E_{cut} of 30 Ry and a $2 \times 2 \times 1$ **k** grid. After the addition of an impurity the system was allowed to fully relax with the same tolerance on the forces as for the clean system of 1×10^{-4} hartrees/bohr. Convergence checks on the values of both E_{cut} and the **k**-point grid were performed, and, crucially, detailed checks were also performed to determine the convergence with respect to supercell size. These checks were performed in the same manner laid out in our previous work [17]. For the 3×3 system size used here we obtained a value of the total energy per atom that was accurate to 1 part in 10^3 when compared to a 3×4 or 4×3 supercell. For E_{cut} we obtained a convergence of the total energy of 2 parts in 10^4 when compared with a calculation run at 34 Ry, and for the **k** grid we obtained a convergence of 1 part in 10^6 when compared to a system with a $3 \times 3 \times 1$ **k** grid.

After relaxation constant-height STM images were calculated using the local density of states (LDOS) of the system following the Tersoff-Hamman model [18],

$$I(V) \propto \int_{E_{\text{BE}}}^{E_{\text{BE}}+eV_{\text{bias}}} \rho_{\text{LDOS}}(\mathbf{r}, E) dE, \tag{1}$$

where ρ_{LDOS} is the local density of states, E_{BE} is the band-edge energy, and V_{bias} is the applied bias voltage. For filled-state imaging we took E_{BE} to be the energy of the highest occupied state, and for empty-state imaging we took E_{BE} to be the energy of the lowest unoccupied state. V_{bias} is +1 eV for empty-state imaging and −1 eV for filled-state imaging. In all our calculations we took the tip position **r** to be 4 Å above the unperturbed surface arsenic positions.

As well as checking the convergence of the total energy, the calculated STM images generated with the different system parameters were compared. We found that there was no discernible change in the images when increasing either E_{cut}, the system size, or the number of points in the **k** grid. For example, going from a 3×3 to a 3×4 supercell changes the peak positions by less than 0.04 Å and the peak intensities by less than 1.5%.

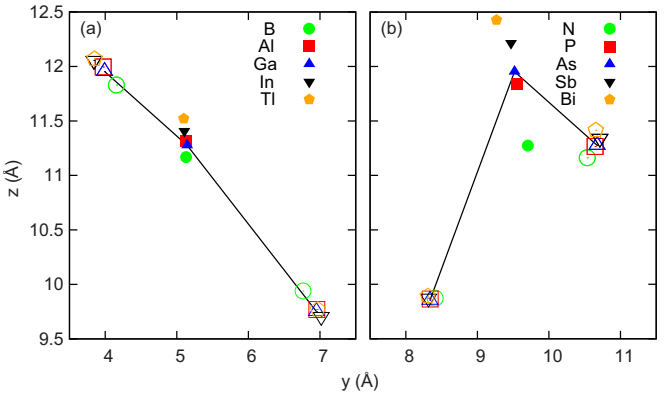

FIG. 1. Side-on view of the final relaxed positions of (a) the group-III and (b) the group-V impurities as well as their first nearest neighbors. Impurity atoms are represented by solid shapes, and the nearest-neighbor atoms are represented by the corresponding open shapes. Bonds are depicted as a guide for the eye.

III. SIGNIFICANCE OF GEOMETRY

A. Overview of DFT results

We find that the final relaxed positions of the dopants change systematically with the position of the dopant in the column of the periodic table. In Sec. V B we show that the change in relaxed position is directly linked to the distribution of the STM contrast. Because of this link between the STM contrast and the relaxed positions it is important to understand the physics of the surface relaxation.

Figure 1 shows how the relaxed positions of the dopants from both groups III and V depend on the atomic number of the dopant. For all plots the x axis is along the $[1\bar{1}0]$ direction, the y axis is along the [001] direction, and the $z = 0$ plane coincides with the bottom atomic layer of the unrelaxed, clean GaAs slab. The top surface arsenic atoms in the relaxed, clean GaAs slab are at $z = +11.953$ Å.

For group III, boron is the dopant with the lowest atomic number and has relaxed farthest into the surface; this is the same for nitrogen in group V. Thallium and bismuth have the largest atomic numbers in each group, and these are the dopants that have relaxed farthest out of the surface in each case. For the group-III dopants a planar bonding configuration is preferred, with the average bond angle in the yz plane being 168.7°, while for group V a more tetrahedral configuration is seen, with an average bond angle in the yz plane being 92.8°. The general form of these configurations, either planar or tetrahedral, is determined by the number of valence electrons, with the different atomic numbers leading to the spread of positions seen in both cases. Further analysis of the DFT data is presented in Sec. V B.

B. Geometrical interpretation

The covalent bond length between two atoms is known to depend on the positions of the atoms in the periodic table. The covalent bond length between atoms A and B, R_{AB}, can be calculated as a sum of their individual covalent radii, r_A and r_B. The covalent radius provides a measure of the effective size of an atom and generally increases with atomic number within a

TABLE I. Average dopant bond lengths for all group-III and -V atoms taken from the DFT simulations compared with bond lengths calculated from the covalent radii in Ref. [8].

	Bond length (Å)				
	B	Al	Ga	In	Tl
DFT	2.05	2.40	2.37	2.55	2.54
Sum of covalent radii	2.06	2.47	2.45	2.63	2.65
	Bond length (Å)				
	N	P	As	Sb	Bi
DFT	1.89	2.29	2.38	2.56	2.67
Sum of covalent radii	1.95	2.35	2.45	2.64	2.75

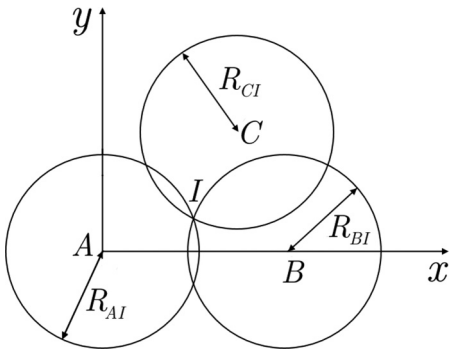

FIG. 2. Two-dimensional diagram of the trilateration procedure (schematic). The bond lengths are taken as the sum of the two covalent radii of the bonded atoms.

group of the periodic table and generally decreases with atomic number across the groups. The length of a covalent bond between any pair of atoms can be estimated from the covalent radii in Ref. [8], which are calculated from experimental data.

In Table I we present a comparison of the average bond lengths from the DFT relaxations for dopants in the surface layer with predicted bond lengths based on the sum of the covalent radius of the dopants and their nearest neighbors. Here we see an increase in bond length in each group and a decrease moving between corresponding dopants going from group III to V. We also see an excellent agreement between the DFT bond lengths and the bond lengths calculated as a sum of the covalent radii, with the largest error being a 4.2% mismatch in the case of thallium. For nitrogen the subsurface relaxation was also investigated (see Sec. V A), and we again found excellent agreement between the predicted and simulated bond lengths, with the second- and third-layer nitrogen dopants having average DFT bond lengths of 2.00 and 2.02 Å, respectively, compared to the sum of the theoretical covalent radii of 1.95 Å. A potential source of the error between the theoretical and DFT bond lengths comes from the pseudopotentials. For the clean GaAs slab our lattice constant is 2.2% smaller than the experimental value, so we expect to see this very slight disagreement in the final bond lengths.

In Fig. 1 dopants of low atomic number tend to relax into the surface, while dopants of high atomic number tend to relax outwards. This is consistent with the tendency for the covalent radii within a group to increase with atomic number, suggesting that geometrical effects, particularly the effective dopant size, are important in these isovalent systems. The covalent radius data also explain the relaxed position of aluminum, which is slightly above the gallium site. This is due to the aluminum atom having a slightly larger covalent radius than gallium, indicating that attributing the trend in relaxed position to atomic number is only an approximation, and the correct driving force behind the relaxation is the effective size of the dopants.

In order to test the idea that the relaxed positions of the dopants depend on their effective size, we have to compute the surface impurity position from the three known lengths of the bonds to the three nearest neighbors. We use a mathematical technique known as trilateration [19], which is a technique used to find a point that is at known distances from three fixed locations. Here the point is the impurity position I, the three fixed locations are the three neighboring atomic positions, A, B, and C, and the known distances are the bond lengths R_{AI}, R_{BI}, and R_{CI}. The three bond lengths trace out spheres centered on A, B, and C, and the impurity position will be at one of the two intersections of these three spheres. Figure 2 illustrates this geometry.

In the case of group V we can approximate the nearest-neighbor positions with the clean-slab positions. In Table II we present the position data for the group-V dopants and their

TABLE II. Comparison of the group-V dopant position and its three nearest neighbors between the DFT simulation and the trilateration calculation. In each case the first line is the dopant position, and the following three lines are the nearest-neighbor positions. For the trilateration positions the three nearest-neighbor positions are the ones used as input to the trilateration procedure. The difference is measured as the Euclidean distance between the two positions.

	DFT positions			Trilateration positions			Difference (Å)
N	5.867	9.708	11.273	5.865	9.752	11.195	0.09
	4.185	10.535	11.163	4.100	10.580	11.180	0.10
	7.548	10.534	11.163	7.631	10.580	11.180	0.10
	5.867	8.408	9.875	5.865	8.337	9.853	0.07
P	5.865	9.552	11.836	5.865	9.521	11.883	0.06
	3.949	10.646	11.266	3.910	10.675	11.276	0.05
	7.781	10.646	11.266	7.821	10.675	11.276	0.05
	5.865	8.341	9.865	5.865	8.337	9.853	0.01
As	5.865	9.520	11.953	5.865	9.418	12.052	0.14
	3.910	10.675	11.276	3.910	10.675	11.276	0.00
	7.821	10.675	11.276	7.821	10.675	11.276	0.00
	5.865	8.337	9.853	5.865	8.337	9.853	0.00
Sb	5.865	9.470	12.216	5.865	9.223	12.372	0.29
	3.837	10.712	11.341	3.910	10.675	11.276	0.10
	7.894	10.712	11.341	7.821	10.675	11.276	0.10
	5.865	8.317	9.873	5.865	8.337	9.853	0.03
Bi	5.865	9.267	12.428	5.865	9.159	12.478	0.12
	3.871	10.654	11.415	3.910	10.675	11.276	0.15
	7.860	10.654	11.415	7.821	10.675	11.276	0.15
	5.865	8.306	9.892	5.865	8.337	9.853	0.05

three nearest neighbors taken from the DFT relaxation and the trilateration procedure. For the trilateration procedure the three neighbors were fixed in their clean-slab positions, and the dopant position was calculated using the covalent radii. The subsurface nearest neighbors show only small deviations from the clean-slab positions, less than 0.08 Å in all cases, and the surface neighbors show a generally larger displacement of between 0.05 and 0.15 Å. For nitrogen, its small covalent radius produces larger shifts in the nearest neighbors during the DFT relaxation, so fixed nearest-neighbor positions cannot be used; instead, the surface nearest neighbors are shifted slightly, while the subsurface neighbor is kept fixed to allow for a trilateration solution. Our interpretation that the geometry is important in the relaxation is supported by the good agreement between the trilateration positions and the DFT relaxation, with the largest difference in position being only 0.3 Å for the tin dopant. This good agreement is obtained *without* any input from the DFT relaxation.

In the case of group III the dopants prefer a planar bonding configuration. In contrast to the tetrahedral preference of the group-V atoms, this causes a greater movement in the nearest neighbors. Because of this we cannot set up the trilateration calculation in a way that is independent of the DFT relaxation. We can, however, test our geometrical interpretation by using the nearest-neighbor positions from the DFT relaxation in the trilateration procedure. Table III shows the group-III dopant positions calculated in this way, along with the DFT positions. We see that the difference in the predicted dopant position and the DFT position is larger than in the case of group V, even when using the DFT positions. This is due to the small difference between the DFT bond length, which comes from the pseudopotentials, and the sum of the covalent radii. These differences are not identical for all bond lengths, with the subsurface bond mismatch being, on average, 1.1% and the surface bond mismatch being, on average, 3.8%. The bond-length difference has a greater influence on the predicted position for the planar geometry than in the case of the tetrahedral geometry of the group-V dopants. The relationship between the difference in position D and the bond angle θ for a 3.8% bond-length mismatch is given by

$$D = R_{\mathrm{DFT}}\left[\sqrt{1.038^2 - \cos^2\left(\frac{180-\theta}{2}\right)} - \sin\left(\frac{180-\theta}{2}\right)\right], \tag{2}$$

where R_{DFT} is the DFT bond length. This expression has a maximum at $\theta = 180^\circ$ and a minimum at $\theta = 0^\circ$. The planar geometry of the group-III dopants gives an average θ of 168.7°, which gives a difference in position of $\sim 0.2 R_{\mathrm{DFT}}$, while the group-V dopants have an average bond angle of 92.8°, which gives a smaller difference in position of $\sim 0.05 R_{\mathrm{DFT}}$. The value of D at 92.8° is small because the function of θ on the right of Eq. (2) stays quite flat far away from the minimum at $\theta = 0^\circ$ and only starts to increase significantly when $\theta \sim 115^\circ$.

These results suggest that the geometrical interpretation does apply to group-III dopants. Once the nearest-neighbor shifts have been accounted for the remaining discrepancy can be explained as a consequence of the planar geometry enhancing the effect of the bond-length errors. To confirm this we perform the same trilateration procedure as before but now with both the DFT bond lengths and positions to obtain the following differences in position: $D_B = 0.01$ Å, $D_{\mathrm{Al}} = 0.01$ Å, $D_{\mathrm{Ga}} = 0.04$ Å, $D_{\mathrm{In}} = 0.02$ Å, and $D_{\mathrm{Th}} = 0.03$ Å, showing the accuracy of the trilateration method once the bond-length errors have been reduced.

The geometrical interpretation therefore applies to both group-III and -V surface-layer dopants. The trilateration method works well in the case of surface impurities in tetrahedral lattices as the impurity has three points of contact with the surface and less well for planar geometries, which enhance the effect of any bond-length errors. For subsurface impurities the relaxation becomes more complicated, involving four bonds, and can no longer be easily predicted with this method.

By using the covalent radius model we obtain bond lengths with an error of less than 4.2% and positions with an average deviation of only 0.19 Å when compared with the full DFT relaxation for all dopants and nearest neighbors. This method was used to seed the DFT relaxation for all the surface dopants in this work allowing for a more efficient relaxation. In the case of bismuth, for example, the number of iterations required to minimize the forces was reduced from 63 to 40.

It is the final position of the different impurities that determines the character of the STM image. From our geometrical model we expect all impurities with a covalent radius smaller than the substituted atom to produce dark regions in the STM image as they move into the surface and impurities with a larger covalent radius than the substituted atom to produce bright regions as they move out. This is true in both the filled-state imaging of group-V impurities and the empty-state imaging of group-III impurities (see Sec. V B).

TABLE III. Comparison between the DFT simulation and the trilateration calculation for the group-III dopant and nearest-neighbor positions. For the DFT positions the first line is the dopant position, and the following three lines are the nearest-neighbor positions. The DFT nearest-neighbor positions are used as input for the trilateration calculations in this case. The difference is measured as the Euclidean distance between the two positions.

	DFT positions			Trilateration positions			Difference (Å)
B	3.910	5.131	11.168	3.910	5.250	11.342	0.21
	3.910	6.760	9.940				
	2.233	4.158	11.830				
	5.588	4.158	11.830				
Al	3.910	5.131	11.318	3.910	5.410	11.696	0.47
	3.910	6.956	9.770				
	1.925	3.970	11.996				
	5.895	3.970	11.996				
In	3.910	5.105	11.408	3.910	5.358	11.745	0.42
	3.910	7.018	9.706				
	1.783	3.843	12.056				
	6.038	3.843	12.056				
Tl	3.910	5.097	11.522	3.910	5.414	11.915	0.59
	3.910	6.970	9.770				
	1.777	3.849	12.069				
	6.043	3.849	12.069				

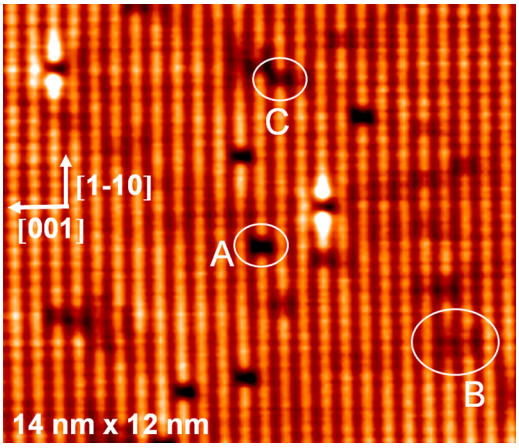

FIG. 3. Constant current height scan of the filled states for a nitrogen-doped GaAs (110) surface reproduced from Ref. [9]. A, B, and C are features due to nitrogen impurities in the first, second, and third atomic layers, respectively.

IV. EXPERIMENTAL RESULTS

The XSTM studied sample consists of three groups of N:GaAs/GaAs quantum wells (QWs) with nitrogen concentrations of $(0.4 \pm 0.1)\%$, $(1.0 \pm 0.1)\%$, and $(2.5 \pm 0.3)\%$. Each group of QWs in turn contains three identical 15-nm-wide QWs that lie 25 nm apart from each other. A detailed description of the sample and the structural characterization of the different QWs of this sample can be found elsewhere [9].

All XSTM measurements were performed with a room-temperature Omicron STM-1 under ultrahigh vacuum conditions ($p < 6 \times 10^{-11}$ mbar) on *in situ* cleaved (110) surfaces. Electrochemically etched polycrystalline tungsten tips were used. The XSTM was operated in constant-current mode at negative sample voltages, giving direct access to the group-V sublattice. In Fig. 3 a typical filled-state XSTM image can be seen, showing three typical nitrogen-related features on the (110) surface originating from nitrogen atoms in the first (A), second (B), and third (C) layers.

V. THEORETICAL RESULTS

A. N:GaAs

LDA DFT simulations were performed for nitrogen impurities in the first three surface layers of GaAs (110). Figures 4(a)–4(c) show the results of our DFT calculations for the first-, second-, and third-layer nitrogen simulations, respectively, while Figs. 4(d)–4(f) show a side-on diagram of the relaxed geometry. We have included the position of the clean surface as well as the clean-surface atomic positions for comparison.

For the first-layer impurity we see a dark region in the calculated STM image above the nitrogen location [Fig. 4(a)]. This dark region is caused by the reduced size of the nitrogen compared to the arsenic atoms, which results in it relaxing into the surface [Fig. 4(d)]. This change of 0.69 Å in the z position of the impurity causes a shift in the tail of the wave function. Outside of the surface the impurity wave function decays exponentially with z, so a small change in z can lead to a very rapid reduction in the LDOS above the nitrogen when compared to the surrounding arsenic atoms. This matches feature A in the experimental data (Fig. 3). In both Figs. 4(a) and 4(d) we see very little geometrical change in the xy plane for the surrounding arsenic atoms, which leaves the rest of the STM image unperturbed.

For the second-layer nitrogen we get a region of reduced intensity over the four arsenic surface sites closest to the nitrogen position [Fig. 4(b)]. There is very little change in the initial nitrogen position, with most of the effect of the

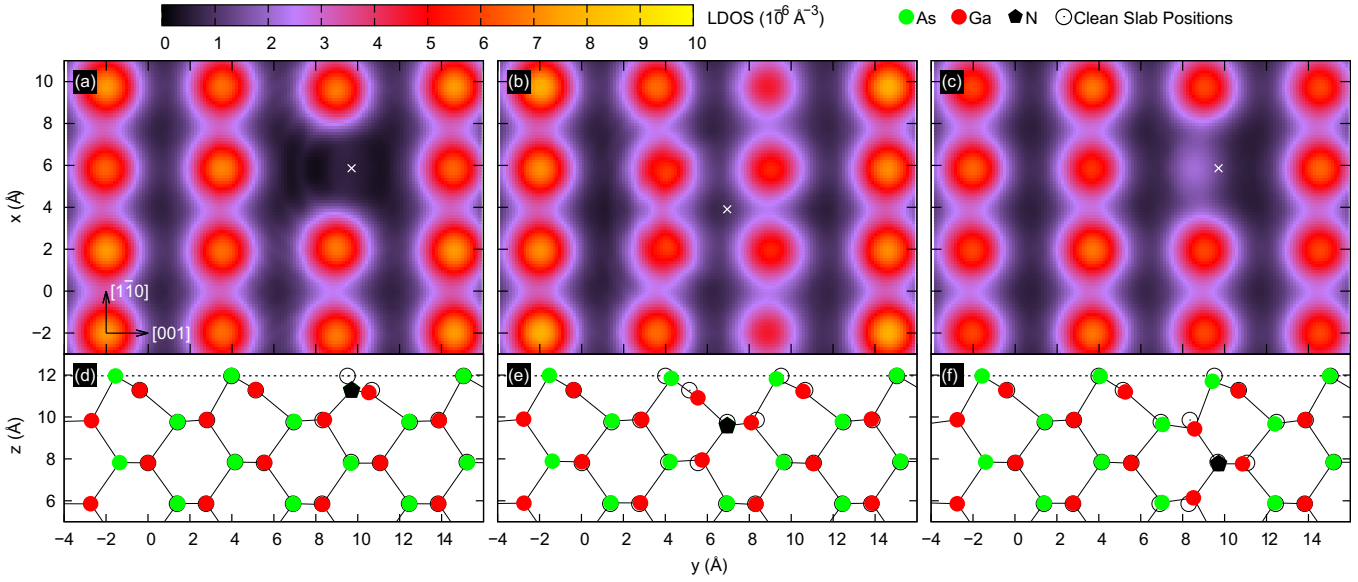

FIG. 4. Comparison of filled-state simulated STM images calculated at a constant height for (a) first-layer, (b) second-layer, and (c) third-layer nitrogen impurities in the GaAs (110) surface layer along with (d)–(f) a diagram of the surface relaxation in each case. In (a), (b), and (c) the position of the nitrogen has been marked with a white cross. In (d), (e), and (f) the gallium and arsenic atoms are shown along with the nitrogen impurity (black pentagon) and the positions of the GaAs atoms for a clean surface (empty circles). The dotted line marks the surface height.

impurity being the shrinking of the bonds to the surrounding atoms [Fig. 4(e)]. This reduction of the N-Ga bond lengths is felt more by the gallium atoms closest to the surface; the ones farther into the slab are surrounded by more bulk structure and so are more resistant to movement. The movement of these surface gallium atoms causes four surface arsenic atoms to move mainly parallel to the surface plane, with a slight displacement into the surface [Fig. 4(e)]. The relaxation of the arsenic atoms into the surface is significantly less in this case than for the first-layer nitrogen, with the average shift in z being only 0.12 Å. This has the effect on the calculated STM image of causing only slight reductions in the LDOS located above those four atoms. This feature, spread over multiple arsenic sites, corresponds to feature B in Fig. 3. The agreement between the theory and experiment for this case is discussed further later in this section.

The third-layer nitrogen produces a very similar feature to the first-layer case: a relatively unperturbed surface with a dark region above the nitrogen site [Fig. 4(c)]. There is an even smaller change in position of the nitrogen away from the initial substitutional position than in the second-layer case, and again we see that most of the response to the nitrogen is a shrinking of the bonds with its nearest neighbors. As with the second-layer case this has the largest effect on the gallium atom closest to the surface [Fig. 4(f)]. The relaxation of this gallium atom close to the surface pulls down the single surface arsenic atom located above it, resulting in a calculated STM image that is very similar to Fig. 4(a). The relaxation in z of the surface arsenic atom in this case is 0.23 Å, which is smaller than in the first-layer case. This relaxation is still large enough to cause a general dark region around the atom, but because the shift is much smaller than the 0.69 Å value for the first-layer case, the intensity in the dark region is almost three times higher than in the first-layer case. This feature caused by the third-layer nitrogen corresponds to feature C in Fig. 3. STM images for nitrogen on GaAs (110) calculated on the basis of DFT were first reported in Ref. [10], but without the geometrical interpretation and quantitative experiment-theory comparison reported here. Although we use pseudopotentials that differ from those used in Ref. [10], our calculated STM images for first-, second-, and third-layer nitrogen impurities agree qualitatively with those in Ref. [10]. The calculated bond lengths are also in reasonable agreement. For example, the N-Ga bond lengths for N in the first layer agree to within 5%.

A feature of interest in the second-layer case is the in-plane shift of the four surface arsenic atoms, as well as slight differences in their peak intensities. In Fig. 5 we compare the data for the second-layer feature from both experiment [Fig. 5(a)] and theory [Fig. 5(b)]. Here the cell dimensions have been scaled and are given in terms of lattice constant a_0. From line scans of the experimental data in Fig. 5(c) we measure an average shift of the positions of the peaks marked at A in the y direction of 8.3% ± 0.8% of the clean arsenic row separation. In Fig. 5(d) we show a line scan of the data taken from our simulations where we measure a shift in the peaks at A of 10% in the y direction of the clean arsenic row separation. The peaks at B are smaller than the peaks at A and are measured experimentally to have an average shift of 2.6% ± 0.7%, while the simulation gives a shift of 2.5%. In the experimental data

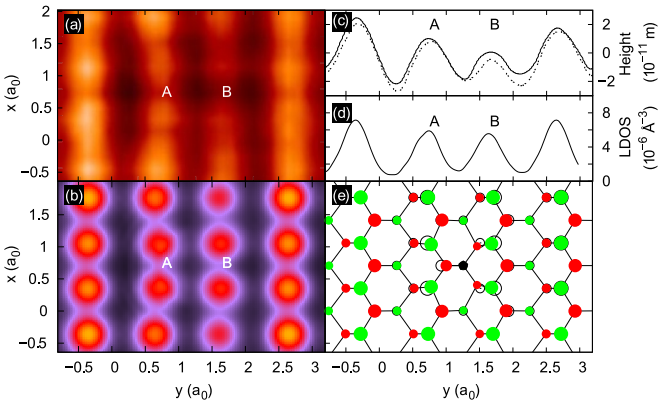

FIG. 5. Theoretical and experimental STM data for a second-layer nitrogen feature. (a) Constant current experimental STM data taken from Fig. 3 (the image has been flipped horizontally to line up with the geometry of the simulation), (b) simulated constant height STM image [repeated from Fig. 4(b)], (c) line scans of experimental data showing the relative peak heights with the dotted line being taken from (a) at $x \approx 1.1$ and the solid line taken from (a) at $x \approx 0.4$, (d) line scan of simulation data taken from (b) at $x = 0.37$, and (e) diagram of the DFT surface relaxation in the (110) plane. In (e) the dots are scaled depending on their distance away from the surface.

there is a slight asymmetry between the two shifts at A as well as an asymmetry of the two shifts at B [Fig. 5(c)], while in the simulation both shifts at A are symmetric and so are those at B. This is thought to be due to the inhomogeneity of the surrounding area in the experimental sample, compared to the perfectly periodic system in the simulation.

The difference in both shift and intensity of the two peaks at A and the two at B can be explained by the geometry of the surface and position of the nitrogen impurity. In Fig. 4(e) we see that the nitrogen atom's neighboring gallium atom that is closer to the surface has a larger displacement than the other neighboring atoms. This gallium is only fixed to the surface through three bonds while the other neighbors have four. This allows it to move more in response to the addition of the nitrogen impurity, which in turn leads to a large movement in the two surface arsenic atoms bonded to it. The difference in intensities comes from the fact that the pair of arsenic atoms at A is being pulled parallel to the surface due to the position of their neighboring gallium, while the two arsenic atoms at B are mainly being pulled down into the surface. These two effects are seen in the image as the two peaks at A having a larger in-plane shift in position while the peaks at B have a smaller shift but a larger reduction in intensity.

B. Group-III and -V isoelectronic impurities

The behavior of the nitrogen dopant in the first three surface layers of GaAs can be understood as a simple consequence of the difference in effective sizes between the nitrogen and the arsenic atoms. Predictions can be made based on our geometrical model on how other isovalent impurities will behave in GaAs and what would be seen in the resulting STM images. As explained previously, our model predicts that any impurities with a smaller covalent radius than the atoms they substitute will cause darker regions in the STM images,

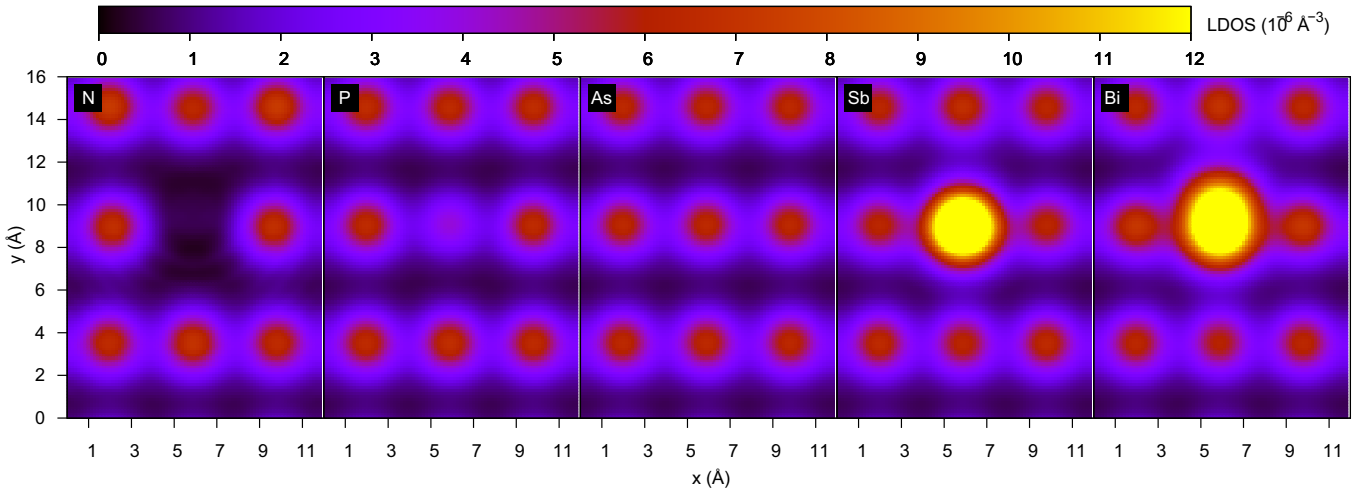

FIG. 6. Simulated filled-state STM images at constant height for group-V impurities on the first layer of the GaAs (110) surface: nitrogen, phosphorus, arsenic, antimony, and bismuth. The increasing effective size of the impurities directly relates to the change in the intensity of the image over the impurity site.

whereas impurities that are larger than the substituted atom will cause brighter regions. To test this a range of impurities in the first layer of a GaAs (110) slab was simulated. The impurities investigated were those from groups III, boron, aluminum, indium, and thallium, and those from group V, phosphorus, antimony, and bismuth, which, when combined with the results of nitrogen as well as the clean GaAs surface, provide a full picture of both groups of isovalent impurities.

1. Group-V STM images

Figure 6 shows the series of simulated filled-state STM images generated for the five group-V atoms on the (110) surface. The increasing effective size of the impurities down the group moves the relaxed position from below the surface in the case of nitrogen, all the way up through the surface layer ending with bismuth at the highest position. This is seen in the calculated STM images as a change in the intensity of the image over the dopant site with dark contrast over N and P atoms, which relax into the surface, and bright contrast over Sb and Bi atoms, which relax out of the surface.

The empty-state images for the group-V impurities are shown in Fig. 7. For the phosphorus and arsenic systems there is no noticeable change in the image due to the minimal relaxation. For the nitrogen case the neighboring gallium atoms have relaxed inwards, with each peak having moved away from the clean position by around 0.44 Å. This results in a redistribution of their empty states in the calculated STM image, as seen in Fig. 7. This relaxation also causes the gallium atoms at the edges of the supercell to be forced up slightly as the ones in the middle are pulled down. For antimony and bismuth, the impurity atoms are far enough out of the surface that their associated empty states have not decayed away in strength as much as the surrounding gallium states and so have a sizable presence in the image above the impurity location.

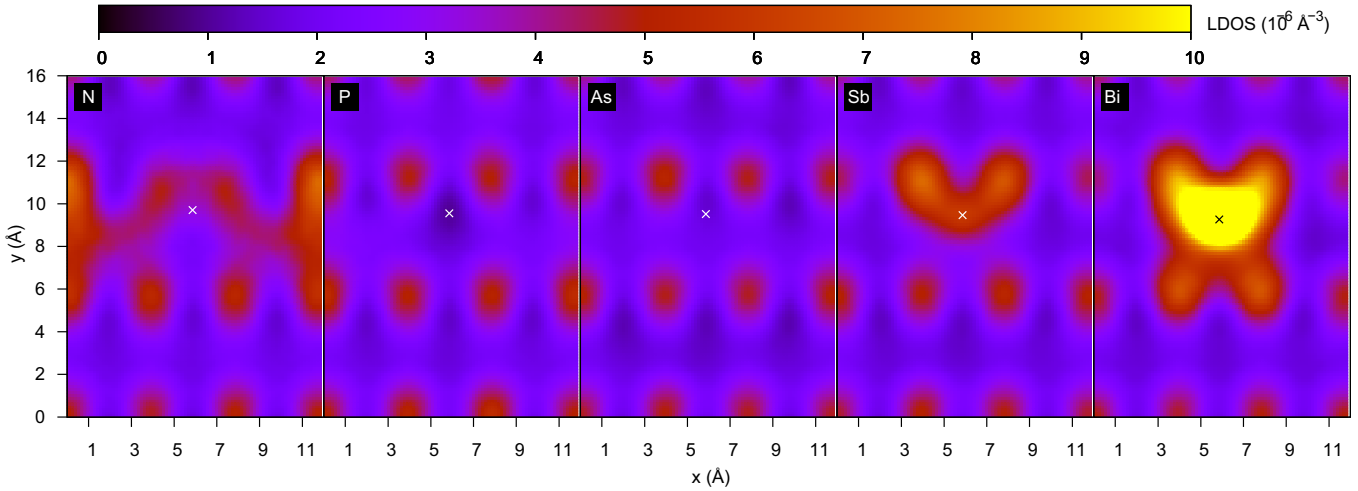

FIG. 7. Simulated empty-state STM images at constant height for group-V impurities on the first layer of the GaAs (110) surface: nitrogen, phosphorus, arsenic, antimony, and bismuth. The impurity location in each case is marked with a cross.

All group-V isoelectronic dopants that have been studied theoretically in this paper have been observed experimentally by XSTM. In all cases the calculated contrast corresponds nicely to the experimentally observed contrast at filled-state imaging conditions. There is also promising agreement for both N and Sb in empty-state imaging conditions.

XSTM images show that N-doped GaAs [9,20] gives rise to a dark contrast on top of the N atom. Reference [20] also shows weak bright contrast for empty-state images of nitrogen, which agree qualitatively with the results of the simulation shown in Fig. 6. The experimentally observed filled-state contrast on P atoms in P-doped GaAs [21] shows the same dark contrast predicted by the simulations. In the case of Sb-doped GaAs, the XSTM experiments show the predicted bright contrast on Sb atoms for both filled- and empty-state imaging [22] (see Figs. 6 and 7), as is the case for filled-state imaging of Bi-doped InP material [23].

2. *Group-III STM images*

Figure 8 shows the series of empty-state simulated STM images for the group-III atoms on the (110) surface. As in Fig. 6, the increasing effective size of the impurities down the group has the boron impurity below the surface level while indium and thallium atoms, which are of greater effective size, are above the surface. This has the effect on the calculated STM image of causing a dark area in the LDOS over the boron site and bright areas over the indium and thallium sites. The effect of the slightly increased effective size of aluminum compared to gallium can be seen as a small increase of about 14% in the LDOS over the aluminum site compared to that of the gallium.

Because the group-III impurities are farther into the surface than the surrounding arsenic atoms, we see a sizable movement in the relaxation of these surface arsenic atoms. This also has the result of altering the simulated filled-state STM images, which are shown in Fig. 9. Here we are seeing the movement of the arsenic states due to the relaxation of the surface around the impurity. In Fig. 9 the small effective size of the boron impurity has pulled the two neighboring surface arsenic atoms towards each other into the surface. This has the effect of merging the features above these two atoms as well as reducing their intensities by about 20%. In this case the two peaks have each shifted by around 0.44 Å towards each other in x. For the impurities with larger covalent radii such as indium and thallium the neighboring arsenic atoms get pushed away from each other, widening the space between the peaks in the image. For both cases the peaks near the impurity site have each moved away in x by about 0.22 Å.

For group III, the elements Al and In have been frequently observed in GaAs by XSTM due to the popularity of the GaAs/AlGaAs and InAs/GaAs multilayer structures. However, although B-doped [24] and Tl-doped GaAs [25] have been grown, these materials are still hardly studied and have not been explored by STM as far as we know.

For indium, typically, a bright contrast is observed in empty-state imaging conditions [20,26–28], and for filled-state imaging at low indium concentrations there appears to be no indium contribution to the image [20]. This agrees with our simulations, which also show a bright contrast in the empty-state imaging and no indium contrast in the filled-state images. Some experimental results for indium in GaAs disagree with this and show bright spots in the filled-state imaging [28,29]; however, these results typically contain samples with very high concentrations of indium or are for systems with very high lattice strain such as quantum dots or rings.

In empty-state imaging conditions a weak dark contrast is typically seen for Al in $Al_xGa_{1-x}As$ [30,31], but this is not reproduced in the simulations. For the majority of group-III dopants the large difference in effective size between the dopant and the Ga atom that it substitutes determines the physics and hence the contrast in the STM images. However, as Al is very similar to Ga in effective size, more subtle electronic effects may also play a role in determining the weak contrast. In this case the experiments in Refs. [30,31] may not be directly comparable to our calculations: in the experiments where the aluminum fraction is very high ($x \geqslant 0.3$) we would expect

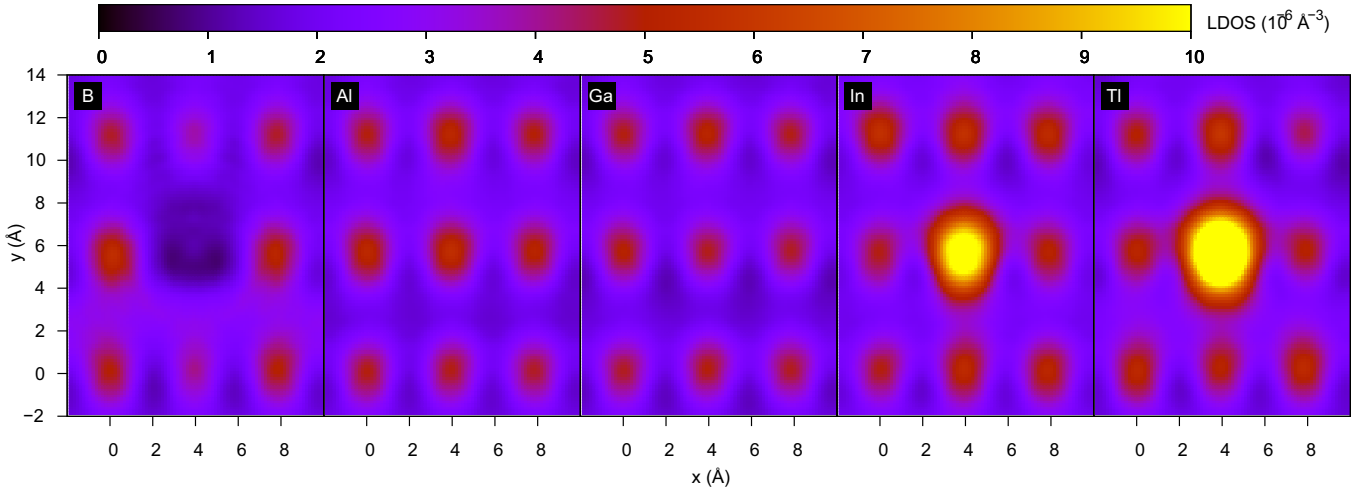

FIG. 8. Empty-state calculated STM images at constant height for group-III impurities on the first layer of the GaAs (110) surface: boron, aluminum, gallium, indium, and thallium. We see that the smallest atom, boron, leaves a dark region in the image due to it moving into the surface. The impurities bigger than gallium relax outwards and so give brighter spots. The similarity between the aluminum and gallium images comes from the two dopants having almost identical covalent radii and thus relaxations.

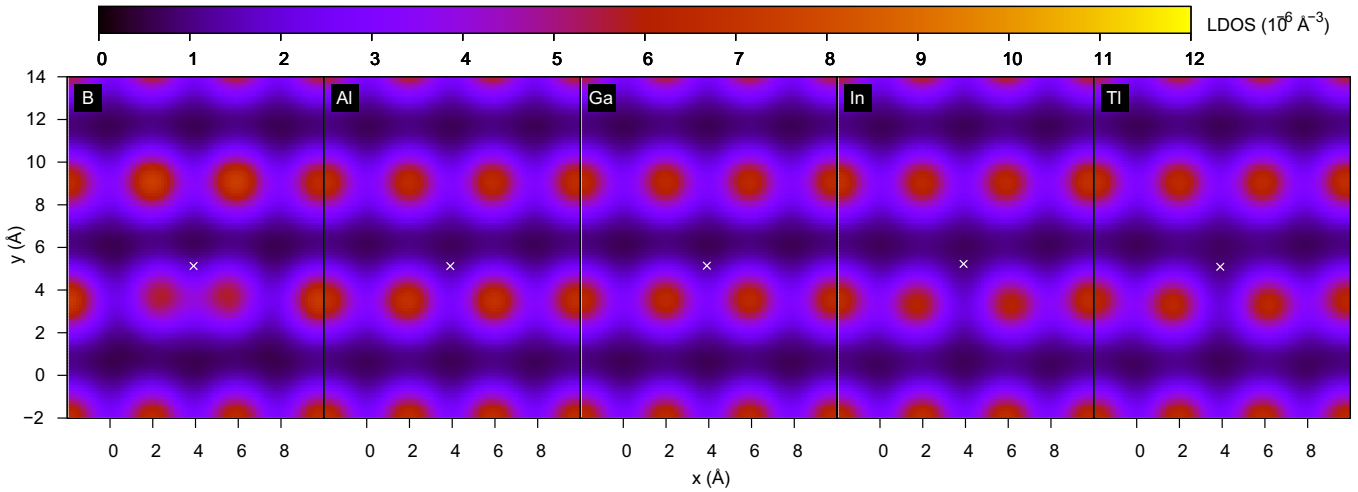

FIG. 9. Simulated filled-state STM images at constant height for group-III impurities on the first layer of the GaAs (110) surface: boron, aluminum, gallium, indium, and thallium. The boron system shows a moving together of the nearest arsenic atoms due to the small effective size of the impurity. The larger indium and thallium impurities push the arsenic atoms away, introducing a space near the impurity location. The relaxed position of the impurity in each simulation has been marked with a white cross.

much larger electronic interactions between Al atoms than are present in our simulation where $x = 0.016$.

VI. SUMMARY

In this work we have shown that the behavior and appearance of nitrogen features on the GaAs (110) surface can be explained primarily through a simple analysis of the geometry of the system. This behavior has been verified through LDA DFT simulations and compared to experimental results. We find good qualitative agreement between the calculated and experimental STM images, and in cases where atomic shifts can be measured we find excellent quantitative agreement. Extending this analysis, we find that the effective size of the impurity and the system geometry are the main influence on the STM images for all the isovalent impurities studied. All atoms from groups III and V behave in a predictable manner based on their effective sizes, which gives rise to clear trends in the relaxations and STM images. We have shown that the effect of the group-V (group-III) impurities is also visible through empty- (filled-) state imaging.

[1] C. Kurtsiefer, S. Mayer, P. Zarda, and H. Weinfurter, Phys. Rev. Lett. **85**, 290 (2000).
[2] K. Y. Tan, K. W. Chan, M. Möttönen, A. Morello, C. Yang, J. van Donkelaar, A. Alves, J. Pirkkalainen, D. N. Jamieson, R. G. Clark, and A. S. Dzurak, Nano Lett. **10**, 11 (2010).
[3] R. Vrijen, E. Yablonovitch, K. Wang, H. W. Jiang, A. Balandin, V. Roychowdhury, T. Mor, and D. DiVincenzo, Phys. Rev. A **62**, 012306 (2000).
[4] B. Nosho, W. Barvosa-Carter, M. Yang, B. Bennett, and L. Whitman, Surf. Sci. **465**, 361 (2000).
[5] A. M. Yakunin, A. Y. Silov, P. M. Koenraad, J. H. Wolter, W. Van Roy, J. De Boeck, J.-M. Tang, and M. E. Flatté, Phys. Rev. Lett. **92**, 216806 (2004).
[6] J. H. Davies, D. M. Bruls, J. W. A. M. Vugs, and P. M. Koenraad, J. Appl. Phys. **91**, 4171 (2002).
[7] B. Grandidier, Y. M. Niquet, B. Legrand, J. P. Nys, C. Priester, D. Stiévenard, J. M. Gérard, and V. Thierry-Mieg, Phys. Rev. Lett. **85**, 1068 (2000).
[8] P. Pyykkö and M. Atsumi, Chem. Eur. J. **15**, 186 (2009).
[9] J. M. Ulloa, P. M. Koenraad, and M. Hopkinson, Appl. Phys. Lett. **93**, 083103 (2008).
[10] X. Duan, M. Peressi, and S. Baroni, Phys. Rev. B **75**, 035338 (2007).
[11] ABINIT, http://www.abinit.org/downloads/psp-links/psp-links/lda_fhi.
[12] X. Gonze *et al.*, Comput. Phys. Commun. **180**, 2582 (2009).
[13] X. Gonze, J.-M. Beuken, R. Caracas, F. Detraux, M. Fuchs, G.-M. Rignanese, L. Sindic, M. Verstraete, G. Zerah, F. Jollet, M. Torrent, A. Roy, M. Mikami, Ph. Ghosez, J.-Y. Raty, and D. C. Allan, Comput. Mater. Sci. **25**, 478 (2002).
[14] G.-X. Qian, R. M. Martin, and D. J. Chadi, Phys. Rev. B **38**, 7649 (1988).
[15] Z. Yi, Y. Ma, and M. Rohlfing, J. Phys. Chem. C **115**, 23455 (2011).
[16] P. A. Schultz and O. A. von Lilienfeld, Modell. Simul. Mater. Sci. Eng. **17**, 084007 (2009).
[17] F. J. Tilley, M. Roy, and P. A. Maksym, J. Phys. Conf. Ser. **526**, 012009 (2014).
[18] J. Tersoff and D. R. Hamann, Phys. Rev. B **31**, 805 (1985).
[19] E. Doukhnitch, M. Salamah, and E. Ozen, Comput. Commun. **31**, 4124 (2008).
[20] H. A. McKay, R. M. Feenstra, T. Schmidtling, U. W. Pohl, and J. F. Geisz, J. Vac. Sci. Technol. B **19**, 1644 (2001).

[21] A. Lew, C. Yan, C. Tu, and E. Yu, Appl. Phys. Lett. **67**, 932 (1995).

[22] R. Timm, R. M. Feenstra, H. Eisele, A. Lenz, L. Ivanova, E. Lenz, and M. Dähne, J. Appl. Phys. **105**, 093718 (2009); R. Timm, A. Lenz, H. Eisele, L. Ivanova, M. Dähne, G. Balakrishnan, D. L. Huffaker, I. Farrer, and D. A. Ritchie, J. Vac. Sci. Technol. B **26**, 1492 (2008).

[23] C. M. Krammel, P. M. Koenraad, F. J. Tilley, M. Roy, P. A. Maksym, K. Wang, and S. M. Wang (unpublished).

[24] M. Groenert, R. Averbeck, W. Hösler, M. Schuster, and H. Riechert, J. Cryst. Growth **264**, 123 (2004).

[25] R. Beneyton, G. Grenet, P. Regreny, M. Gendry, G. Hollinger, B. Canut, and C. Priester, Phys. Rev. B **72**, 125209 (2005).

[26] J. F. Zheng, J. D. Walker, M. B. Salmeron, and E. R. Weber, Phys. Rev. Lett. **72**, 2414 (1994).

[27] P. Offermans, P. M. Koenraad, R. Nötzel, J. H. Wolter, and K. Pierz, Appl. Phys. Lett. **87**, 111903 (2005).

[28] M. Pfister, M. B. Johnson, S. F. Alvarado, H. W. M. Salemink, U. Marti, D. Martin, F. Morier-Genoud, and F. K. Reinhart, Appl. Phys. Lett. **67**, 1459 (1995).

[29] D. Bruls, P. Koenraad, M. Hopkinson, J. Wolter, and H. Salemink, Appl. Surf. Sci. **190**, 258 (2002).

[30] H. Salemink, M. Johnson, and O. Albrektsen, J. Vac. Sci. Technol. B **12**, 362 (1994).

[31] A. Smith, K. Chao, C. Shih, Y. Shih, and B. Streetman, Appl. Phys. Lett. **66**, 478 (1995).